

Photonic Torque Microscopy of the Non-Conservative Force Field for Optically Trapped Silicon Nanowires

A. Irrera,^{†,#} A. Magazzù,^{†,#} P. Artoni,^{‡,@} S. H. Simpson,[¶] S. Hanna,[§] P. H. Jones,^{||}
F. Priolo,^{‡,⊥} P. G. Gucciardi,[†] and O. M. Maragò^{*,†}

*CNR-IPCF, Istituto per i Processi Chimico-Fisici, I-98158 Messina, Italy, MATIS
CNR-IMM and Dipartimento di Fisica, Università di Catania, I-95123, Catania, Italy,
Institute of Scientific Instruments of the CAS, v.v.i. Czech Academy of Sciences, 612 64
Brno, Czech Republic, H. H. Wills Physics Laboratory, University of Bristol, BS8 1TL
Bristol, UK, Department of Physics and Astronomy, University College London, WC1E
6BT London, UK, and Scuola Superiore di Catania, I-95123 Catania, Italy*

E-mail: marago@ipcf.cnr.it

KEYWORDS: **Optical tweezers, silicon nanowires, non-equilibrium dynamics, Brownian motion**

Abstract

*To whom correspondence should be addressed

†CNR-IPCF

‡MATIS CNR-IMM and Università di Catania

¶ISI-CAS

§University of Bristol

||UCL

⊥Scuola Superiore di Catania

#These authors contributed equally to the work.

@Current address: Center for Life Science, Boston Children's Hospital, Harvard Medical School, Boston, USA

We measure, by photonic torque microscopy, the non-conservative rotational motion arising from the transverse components of the radiation pressure on optically trapped, ultra-thin silicon nanowires. Unlike spherical particles, we find that non-conservative effects have a significant influence on the nanowire dynamics in the trap. We show that the extreme shape of the trapped nanowires yields a transverse component of the radiation pressure that results in an orbital rotation of the nanowire about the trap axis. We study the resulting motion as a function of optical power and nanowire length, discussing its size scaling behavior. These shape-dependent non-conservative effects have implications for optical force calibration and optomechanics with levitated non-spherical particles.

Optical tweezers^{1,2} (OT) are tools that use a strongly focused laser beam to trap and manipulate microscopic³ and nanoscopic⁴ materials. At the nanoscale OT are used for the manipulation,⁵⁻¹⁰ assembly,^{11,12} and characterization¹³⁻¹⁵ of individual nanostructures, as well as probes in photonic force microscopy applications.¹⁶⁻¹⁸ Recently, the possibility to investigate the structural,¹⁴ optical,^{16,19} and thermal^{20,21} properties of individual nanowires in OT has been at the core of intense research. In this context, their extreme shape has a key role in determining their properties as well as optical forces^{22,23} and dynamical stability²⁴ against thermal fluctuations in OT. Silicon nanowires (SiNWs) are an important material for applications in microelectronics, photonics, and photovoltaics.²⁵ Recent experiments have also shown great potential for photodynamic²⁶ therapy applications, as optically trapped SiNWs can photosensitize singlet-oxygen, as well as photothermal²⁰ therapy when ion-implanted to increase photothermal heating. Hence, the opportunity to understand and accurately control the position and orientation of individual SiNW can open perspectives for all those fields.^{4,25}

The origin of optical forces in OT is readily explained in the two limiting cases of spherical particles that are either much smaller^{27,28} (dipole approximation) or much larger^{29,30} (ray optics) than the trapping wavelength. In these two extreme regimes, the force divides into two

main contributions:² a conservative force proportional to the gradient of the light intensity that is responsible for trapping, and a non-conservative scattering force directed along the light beam propagation direction and proportional to the light intensity that generally has a destabilizing effect for optical trapping.

It is a general result of vector calculus (Helmholtz theorem) that any well-behaved vector field can be always decomposed into the sum of a non-rotational (curl-free) component and a rotational (divergence-free) component.³¹ Thus, any generic optically trapped particle can be considered to be subject to a force that is the sum of a conservative and a non-conservative term:^{32,33}

$$\mathbf{F} = -\nabla U + \nabla \times \mathbf{A} \quad (1)$$

The first term represents the conservative force arising from the gradient of an effective trapping potential. The second term represents the non-conservative force (\mathbf{F}_{NC}) related to the components of the radiation pressure.³⁴⁻³⁶ For spherical particles, the non-conservative term arises mainly from the longitudinal radiation pressure related to the inhomogeneous **Gaussian** laser beam used to create OT.^{33,37} This is responsible for a rotational motion coupling to the Brownian dynamics of trapped particles in the directions transverse (ρ) and parallel (z) to the beam propagation direction^{33,38-40} (the ρ - z plane in Fig. 1). For non-spherical particles, however, the situation is much more complex. First, the traditional identification of intensity gradient and scattering force is not generally applicable.⁴¹ Second, the non-spherical shape results in transverse radiation pressure components³⁴ that can have dramatic consequences for the particle's dynamics. First outlined in an astrophysical context to explain the dynamics of interstellar dust,⁴² these radiation force components depend critically on the orientation of a non-spherical particle along the light propagation (axial) direction and generate phenomena such as the "optical lift effect"^{43,44} or the tumbling and rotational motion of micro-ellipsoids^{45,46} and nanofibers.⁷

Here, we report measurements on non-conservative rotations at the nanoscale, performed by means of photonic torque microscopy⁴⁷ (PTM) on optically trapped silicon nanowires.

We show how non-conservative effects scale with laser power and nanowire length, finding that they have a significant role in the nanowire thermal dynamics. We show that the extreme shape of the trapped nanosystem yields a transverse component of the radiation pressure that drives an orbital rotation of the nanowire about the trap axis. Finally we estimate the non-conservative torque, and the work extracted by thermal fluctuations from the non-conservative transverse component of the radiation force.

The geometry of the problem under study is shown in Fig. 1. In Fig. 1a we consider a single nanowire confined and aligned in an OT. The conservative component of the optical force pulls the particle towards the focal region. The coordinate system is fixed at the trap center in the proximity of the focus, and at equilibrium the nanowire main axis is aligned with the trap (z -)axis (see the images in Fig. 1b). **Note that the nanowire center-of-mass position on the optical axis is determined by the nulling of all the forces acting on the nanowire, i.e., axial gradient force, scattering forces, and gravity. At variance with other experiments on thicker nanowires,^{7,11,13} our ultra-thin nanowires are pushed upwards with respect to the focal point only by a fraction of their length (about 10-20%) by the longitudinal radiation pressure (see Supplementary Information).** Figure 1c shows the conservative component of the optical force acting on a trapped SiNW during a rotational motion in the ρ - z plane. To test its conservative nature we consider a predetermined closed path, then we split this path in four parts and calculate the work done on each part (connecting points 0 – 3 in Fig. 1c). On the paths 0 – 1 and 2 – 3, the work is zero since the gradient force is perpendicular to the particle path. On the path 1 – 2 and 3 – 0, work is different from zero, since the force changes parallel to the path, but has opposite sign. By summing up the work carried out in each path we verify that the work is null. This is valid regardless of the path chosen. We now consider the non-conservative components, i.e., the longitudinal and transverse radiation pressure. Because of the inhomogeneous gaussian intensity, the first one generates a rotational bias field in the ρ - z plane (Fig. 1d). The second non-conservative component is generated by a misalignment of the SiNW with respect to the z axis (Fig. 1e,f). The transverse component

does not produce work along a closed path in the ρ - z plane (Fig. 1e), but gives rise to a roto-translation orbital motion of the SiNW in the x-y plane (Fig. 1f).

In our experiments, ultrathin silicon nanowires^{8,48,49} (SiNWs) are prepared starting from p-type Si single crystal. A discontinuous thin film of nanometric gold is deposited on the samples by electron beam deposition at room temperature using a source of high purity gold pellets^{48,50} (see Supplementary Information). Finally, samples are etched at room temperature in an aqueous solution of HF and H₂O₂ to form SiNWs. Note that our samples have a photoluminescence spectrum in the visible range^{48,50} that can be excited with ultraviolet or visible light. However, at our trapping wavelength, 830 nm, no photoluminescence is excited at the available power in the trap, and the nanowires have the dielectric properties of bulk silicon.⁸ Figure 1b shows a typical cross section SEM image of SiNWs obtained after the wet etching of the Au-covered Si substrates. The image displays a dense and uniform distribution of nanowires, having the same length of about 2 μ m. For optical trapping experiments SiNWs with diameter, d , of about 10 nm and different length, L , in the range 1 – 5 μ m are used.⁸ The final step of the SiNWs sample preparation consists in the mechanical scratching of the substrate with a consequent dispersion by sonication in aqueous solution.

Optical trapping experiments are carried out using a near infra-red (NIR) laser diode with wavelength $\lambda = 830$ nm that delivers about 24 mW at the sample. The linearly polarized laser beam is tightly focused by a high numerical aperture microscope objective (NA=1.3, 100 \times) in an inverted configuration. At this wavelength the absorption coefficient of water is negligible^{2,51} (a tenth of that at 1064 nm) and therefore related water heating effects may safely be ignored at our trapping power. Moreover, silicon is a low absorber in the NIR and we expect to have negligible heating effects for ultra-thin native SiNWs optically trapped in water despite their reduced intrinsic thermal conductivity.⁵² Note that in the case of thicker SiNWs some temperature effects and temperature gradients might be present²⁰ and would result in convective flow along the axial direction that would eventually shift upwards the nanowire center-of-mass as well as increasing its thermal dynamics in the trap.

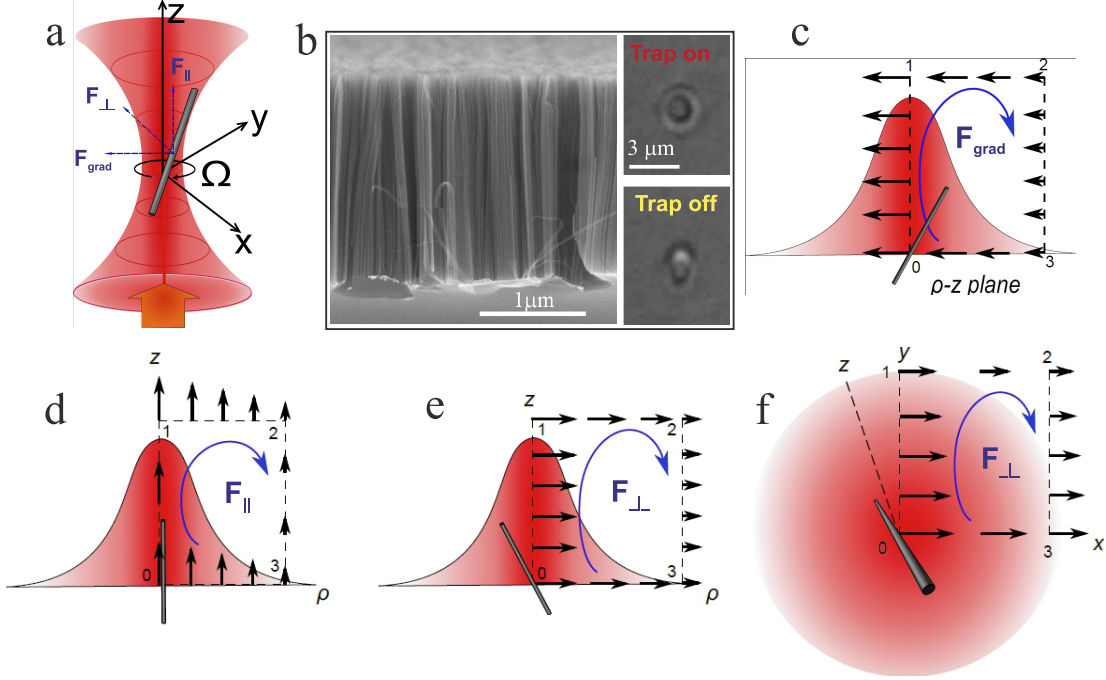


Figure 1: (a) Sketch of a SiNW in an optical trap. Trapping occurs when the gradient force (F_{grad}) overcomes the radiation pressure longitudinal (F_{\parallel}) and transverse (F_{\perp}) components. This latter component arises when the SiNW is misaligned from the z axis by thermal fluctuations, and yields a rotational orbital motion about the z axis of the SiNW with a rotational frequency Ω_{xy} . (b) Typical cross section SEM image (left) of SiNWs on substrate as prepared (see Supplementary Information). The image shows a dense and uniform distribution of nanowires with similar length of about $2 \mu\text{m}$. Diffraction-limited images (right) of a SiNW with a length of $\sim 3 \mu\text{m}$ trapped and aligned in the OT (top right) and moving and tilting in water when the laser is off (bottom right). (c) Conservative gradient force component acting on a SiNW around a closed path in the ρ - z plane. The intensity profile is a simplified, collimated Gaussian beam; it increases approaching the center of the beam. The work done in a closed path connecting points 0 – 3 is null as expected. (d) Non-conservative longitudinal radiation pressure component acting on a SiNW parallel to the optical (z -)axis. The inhomogeneous intensity generates a work and a rotational bias in the ρ - z plane. (e) Representation of the transverse radiation force exerted on a misaligned SiNW in the ρ - z plane. The work done on a closed path is zero. (f) Representation of the transverse radiation force in the x - y plane. Here the transverse force generates work on a closed path and gives rise to a roto-translation orbital motion of the SiNW in the x - y plane.

Trapped nanowires are imaged with a CCD camera through the microscope objective (Fig. 1b). The Brownian motion of a trapped nanowire is studied by back focal plane interferometry^{17,53,54} in the forward direction, i.e., the back focal plane of the microscope condenser contains an interference pattern which is relayed to a quadrant photodiode (QPD) in an optically conjugate plane. Signals from the QPD are processed via analog electronics into a three-dimensional (S_x, S_y, S_z) tracking signal and acquired by a PC through an acquisition board. **The linearity range of the tracking signals for nanowires is within the size range of the laser spot defining the optical tweezers,^{13,55} i.e., for our experimental conditions about $\sim 0.8 \mu\text{m}$ in the transverse plane and $\sim 1.5 \mu\text{m}$ in the axial direction. Since the Brownian dynamics of our nanowires occur on a size range that is less than one order of magnitude smaller,⁸ we are well within the linear range of operation of QPD detection.** An accurate analysis of the decay rate of the autocorrelation functions of the tracking signals enables calibration of the conservative components of the optical force and torque confining and aligning the SiNWs in the trap.⁸ In fact, for small displacements the tracking signals from a trapped SiNW contain information on both the center-of-mass and angular tilting fluctuations.¹⁷

The calibration methods of OT assume that for small displacements from equilibrium the restoring force or torque is proportional to the displacement, *i.e.*, OT are usually considered acting as a Hookeian spring with a fixed stiffness.² This condition implies that the optical force-field must be conservative, thereby excluding the possibility of a rotational (non-conservative) component. Radiation pressure forces, however, are intrinsically non-conservative. Spherical particles experience non-conservative effects only when the intensity of the focused laser beam is sufficiently low to allow the sphere to explore a large volume of the effective confining potential. Under these condition the particle presents a thermal motion with a toroidal bias coupling the directions transverse (ρ) and parallel (z) to the beam propagation.^{33,38–40}

For non spherical particles, such as SiNWs, due to their geometry non-conservative ef-

fects are predicted to be first-order and non-vanishing with increasing laser power.⁵⁶ Highly elongated optically trapped SiNWs are oriented close to the axial direction (z -axis) by optical fields^{11,22,57}. During the trapping process the Brownian motion tends to misalign the nanowires from the z -axis, and consequently a transverse component of the radiation pressure is generated.⁴² This transverse component yields a persistent rotational bias in the $x - y$ plane in addition to the toroidal bias coupling the $\rho - z$ directions caused by the inhomogeneous longitudinal radiation pressure.

We characterize the rotational motion of SiNWs in the optical trap by photonic torque microscopy^{38,47,58} (PTM). In particular, in order to highlight the orbital rotational bias in the transverse ($x - y$) plane we consider the normalized differential cross-correlation functions (DCCFs) of the nanowire tracking signals defined as (see Supporting Information):

$$DCCF_{xy}(\tau) = CCF_{xy}(\tau) - CCF_{yx}(\tau), \quad (2)$$

where $CCF_{xy} = \langle S_x(t)S_y(t+\tau) \rangle / \sqrt{\langle S_x^2(t) \rangle \langle S_y^2(t) \rangle}$ represents the normalized cross-correlation function between tracking signals along the x and y axes as a function of lag time, τ . Here we consider normalized DCCFs so that we can compare results from different SiNWs samples and investigate the scaling behavior of the non-conservative effects with length or power. We fit the DCCFs with the solutions of the Langevin equation in a non-homogeneous force field.⁵⁸ The functional form of the fitting used depends on whether rotational bias or thermal fluctuations dominate the motion of the SiNWs (see Supporting Information). In the case that the positional thermal fluctuations prevail over the orbital rotational bias we use a suitably parameterized hyperbolic function that describes the overdamped regime, otherwise we use a sinusoidal fitting function⁵⁸ that describes the rotational regime of the non-conservative nanowire motion. While we observe that for optically trapped SiNWs the non-conservative rotations prevail over fluctuations in the $x - y$ plane, we find that positional fluctuations overdamp the non-conservative rotations in the $\rho - z$ plane. As a

consequence of this, orbital rotations of the SiNWs persist as they are driven by the non-conservative transverse force in whatever sense they start (see Fig. 2a,b). By contrast, the non-conservative effects in $\rho - z$ plane have characteristics similar to those found for spherical particles,^{33,38-40} i.e., they result from the inhomogeneous longitudinal radiation pressure created by the highly focused laser beam (Fig. 1d). Neither of these phenomena would occur in a simple Hookeian spring model of optical trapping and they are the result of non-zero curl in the optical force. Here, we focus on the observations in $x - y$ transverse plane that are intrinsically related to the non-spherical shape and the occurrence of the transverse radiation pressure (Fig. 1f), while the observations in the $\rho - z$ plane are summarized in the Supporting Information.

First, we evaluate the non-conservative contribution to the nanowire motion as a function of trapping laser power. Figures 2a and b show exemplar DCCFs for a SiNW of length $L = 4.0 \pm 0.2 \mu\text{m}$ at two different values of laser power, $P \approx 1$ and $P \approx 14$ mW, respectively. By fitting the DCCFs oscillations we measure the rotational frequency, Ω_{xy} , in the $x - y$ plane. This is used to define the contribution to the dynamics from non-conservative forces as

$$\epsilon_{xy} = \frac{\Omega_{xy}}{\omega_\rho} \quad (3)$$

where:

$$\omega_\rho = \frac{\omega_x + \omega_y}{2} \quad (4)$$

is the average of the autocorrelation functions (ACFs) decay rates in the transverse plane ($x - y$), $\omega_x = k_x/\gamma_\perp$ and $\omega_y = k_y/\gamma_\perp$, obtained from the transverse tracking signals^{8,17} (S_x, S_y). The decay rates are related to the transverse force constants, k_x and k_y , and to the hydrodynamic viscous coefficient, $\gamma_\perp = 4\pi\eta L/(\ln p + \delta_\perp)$, in the direction perpendicular to the SiNW axis^{6,8,59} which is dependent on the nanowire length, L , water dynamical viscosity, η , length-to-diameter ratio, p , and end correction,⁵⁹ δ_\perp . Evident here is the decrease in rotational frequency at higher power from $\Omega_{xy} \approx 18$ rad/s at $P \sim 1$ mW (Fig.2a) to $\Omega_{xy} \approx 11$

rad/s at $P \sim 14$ mW (Fig.2b) arising from the stronger angular confinement of the SiNW to the optical axis. In Fig. 2(c) the non-conservative contribution to the motion, ϵ_{xy} , and the amplitude of the DCCFs oscillations are shown, and unlike spherical particles they are non-zero (despite being small) even at higher trapping power. This behavior emphasizes that although non-conservative effects for optically trapped non-spherical particles scale down dramatically with laser power they cannot be fully neglected. At low power (~ 1 mW) their contribution is much larger due to the reduced axial alignment (larger orientational fluctuations) that allows the SiNW to explore larger angles with respect to the optical (beam propagation) axis, thus yielding a larger transverse radiation pressure component.

Figures 3a and b show the transverse DCCFs obtained for the longest ($\sim 5 \mu\text{m}$) and shortest ($\sim 1 \mu\text{m}$) SiNWs length, respectively. For the longest SiNWs a fourfold decrease in the oscillation frequency of DCCF oscillations is clearly evident, dropping from $\Omega_{xy} \approx 9.7$ rad/s for $L \sim 1 \mu\text{m}$ (Fig.3a) to $\Omega_{xy} \approx 2.6$ rad/s for $L \sim 5 \mu\text{m}$ (Fig.3b). This is a consequence of the stronger alignment with the axial direction for longer nanowires.⁸ This strong decrease is also observed in Fig. 4a that shows the rotational frequency Ω_{xy} as a function of length. Here each point is the mean of about 20 different measurements for each SiNW sample and the uncertainty is the standard deviation from the mean. Thus, the scaling behavior of the rotational frequency, Ω_{xy} , is found to follow a L^{-2} law with SiNW length. The non-conservative contribution, ϵ_{xy} , and the DCCFs amplitude are plotted in figure 3c. While the latter is found to be fairly constant in the length range explored, the non-conservative component is found to decrease with a L^{-1} scaling law (red solid line in Fig. 3c). This observed scaling behavior is justified by the fact that for SiNW longer than the trapping beam Rayleigh range (as is the case for most of our samples) the transverse trapping forces are fairly constant with length.^{8,13,24} Thus, the trap decay rates, $\omega_x = k_x/\gamma_{\perp}$, $\omega_y = k_y/\gamma_{\perp}$, scale as L^{-1} following the scaling of the hydrodynamic coefficient, and since the non-conservative rotation, Ω_{xy} , is found to scale as L^{-2} (Fig. 4a), we consistently find a L^{-1} scaling behavior for the non-conservative contribution, ϵ_{xy} .

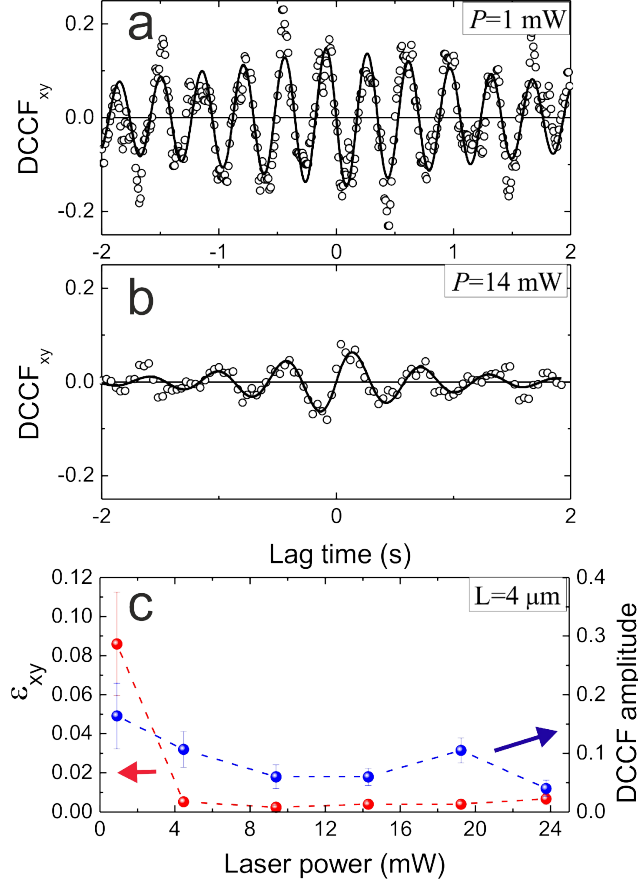


Figure 2: Transverse DCCFs for a SiNW with $L \sim 4 \mu\text{m}$ trapped at two different laser beam powers, $P \approx 1$ mW in (a) and $P \approx 14$ mW in (b). The DCCF oscillation frequency is found to decrease from $\Omega_{xy} = 17.83 \pm 0.03$ rad/s to $\Omega_{xy} = 10.8 \pm 0.1$ rad/s, respectively. Note how the DCCF slope at $\tau = 0$, related to the persistent sense of rotation, in (a) is the opposite of that observed in (b). (c) Non-conservative transverse component of the force field (red) and DCCFs amplitude (blue) as a function of the laser power for a SiNW with $L \sim 4 \mu\text{m}$. About a tenfold increase in the non-conservative component (red data) is observed at low (~ 1 mW) power as the nanowires are subject to larger angular fluctuations that yield a larger radiation pressure transverse component. The error bars represent the standard deviation from the mean value obtained over about 10 measurements for each power value on different trapped nanowires.

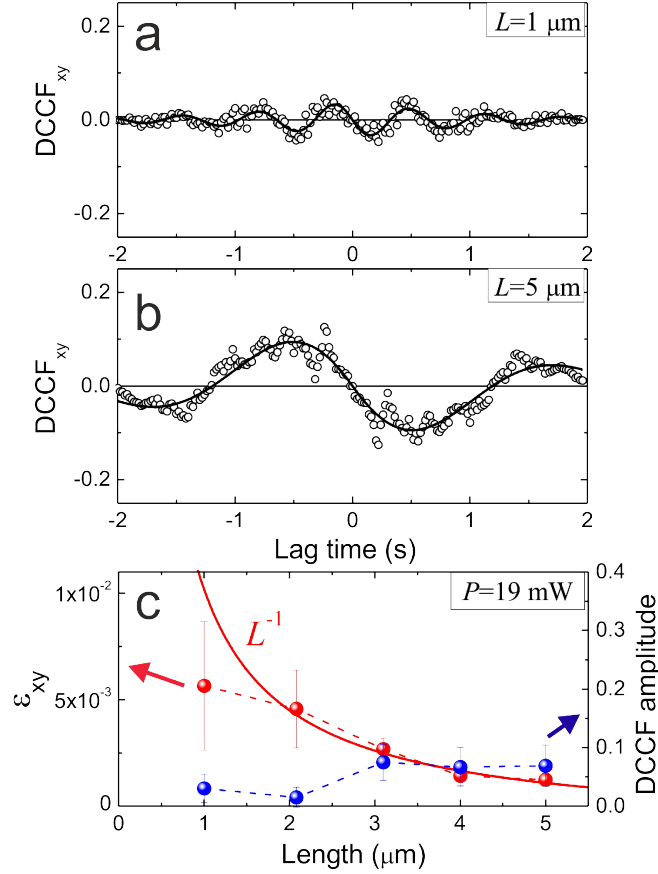


Figure 3: Transverse DCCFs for two different SiNWs trapped at $P \sim 19 \text{ mW}$ with length $L \approx 1 \mu\text{m}$, in (a), and $L \approx 5 \mu\text{m}$, in (b). The DCCF oscillation frequency is found to decrease from $\Omega_{xy} = 9.7 \pm 0.1 \text{ rad/s}$ to $\Omega_{xy} = 2.63 \pm 0.03 \text{ rad/s}$, respectively. (c) Non-conservative transverse component of the force field (red) and DCCFs amplitude (blue) as function of the SiNWs length. The red solid line is an hyperbolic fit representing a L^{-1} size scaling behavior. The error bars represent the standard deviation from the mean value obtained over about 20 measurements for each length.

The slope of the DCCF_{xy} at $\tau = 0$ is related to the sense of rotation of the trapped SiNW. A positive slope is related to a counterclockwise (CCW) circulation of the Brownian vortex with respect to the optical (z -)axis, while a negative slope is related to a clockwise (CW) circulation. In our experiments, from the statistics of all the measurements we observe that about 45% of the time the sense of rotation is negative, hence the circulation is CW, while for the remaining 55% of the times we observe a positive rotation with a CCW circulation. This shows that there is no preferred sense of rotation for long observation times. In fact, the sense of the non-conservative rotational bias is persistent (either positive or negative) in most of our observations within the 2 s acquisition time. However, by breaking the tracks and calculating the DCCFs in subsequent intervals, we were able to observe in a few cases a reversal of the sense of rotation, i.e., a reversal of the DCCFs oscillations (see Sec. S3 in the Supporting Information). This confirms that the observed orbital rotational bias does not come from intrinsic properties of the beam or the SiNWs, but rather depends on averaged orientational (tilting) degrees of freedom (generating the transverse radiation force) that have a much longer relaxation time with respect to the translational ones.^{6,8} While the driving of the process is accounted by the occurrence of the shape-induced transverse force, the initial breaking of the symmetry could arise as the nanowire is pulled into the beam.

The transverse component of the radiation pressure on a SiNW that is tilted with respect to the optical axis generates a non-conservative torque, Γ_{NC} , about the optical (z -)axis (see Fig.1), that yields the non-conservative orbital rotational bias. At equilibrium, the non-conservative radiation torque is counterbalanced by the torque generated by hydrodynamic viscous drag whose modulus is defined as:^{47,58}

$$\Gamma_{\text{drag}} = \gamma_{\perp} \Omega_{xy} \langle \rho^2 \rangle \quad (5)$$

where Ω_{xy} is the rotational frequency in the $x - y$ plane obtained experimentally from the DCCF analysis and $\langle \rho^2 \rangle = \langle x^2 \rangle + \langle y^2 \rangle$ is the measured SiNW mean-squared-displacement in

the transverse plane. Thus, in Fig.4b we show the measured modulus of the non-conservative torque, $\Gamma_{NC,z} = \Gamma_{\text{drag}}$, for the different SiNW samples. Also for this quantity we infer a L^{-1} length scaling from the data that is consistent with the dimensional analysis of $\gamma_{\perp} \propto L$, $\Omega_{xy} \propto L^{-2}$, and the fact that the mean-squared-displacement in the transverse plane is fairly constant for SiNW longer than the trapping beam Rayleigh range.^{8,13,24}

Non-conservative radiation forces acting on the SiNWs cause a thermally activated orbital rotation on the SiNWs about the z -axis and along a nearly circular averaged path. From the details of the path in the transverse plane and the drag force counteracting the non-conservative component, we can estimate the work, \mathcal{W}_{NC} , and the power, \mathcal{P}_{NC} , dissipated by the non-conservative torque in a single rotation:^{38,58}

$$\mathcal{W}_{\text{NC}} = \int_0^{2\pi} \Gamma_{NC,z} d\varphi = 2\pi\gamma_{\perp}\Omega_{xy}\langle\rho^2\rangle \quad (6)$$

$$\mathcal{P}_{\text{NC}} = \Gamma_{NC,z}\Omega_{xy} = \gamma_{\perp}\Omega_{xy}^2\langle\rho^2\rangle. \quad (7)$$

Thus, from our measurements shown in Fig. 4, we can estimate that the work done by the non-conservative force is in the range $\mathcal{W}_{\text{NC}} \approx 0.3 - 1 \times 10^{-22}$ J, while the power dissipated in a cycle is within the range $\mathcal{P}_{\text{NC}} \approx 0.3 - 7 \times 10^{-22}$ W. Note that these work values are about one hundredth of the work done for untwisting DNA,⁶⁰ or four orders of magnitude smaller than the work done by bacterial flagellar motors,⁶¹ as the transverse radiation force component in our experiments is only a fraction in the order of a few percent of the optical force exploited for force or torque transduction with OT.² In this context, understanding how to marshal and control non-conservative optical forces at the nano-scale could help us to power future nano-machines.⁶²

We test these estimates with calculations of the work based on simulations of optical forces on SiNWs by the coupled dipole method²⁴ (see Sec. S4 of the Supporting Information). First we apply a particular tilt and direction to the nanowire, next we calculate the work done, $\mathcal{W} = \oint \mathbf{F} \cdot d\mathbf{r}$, as the wire is translated about a circular loop in the $x - y$ plane, centered at the

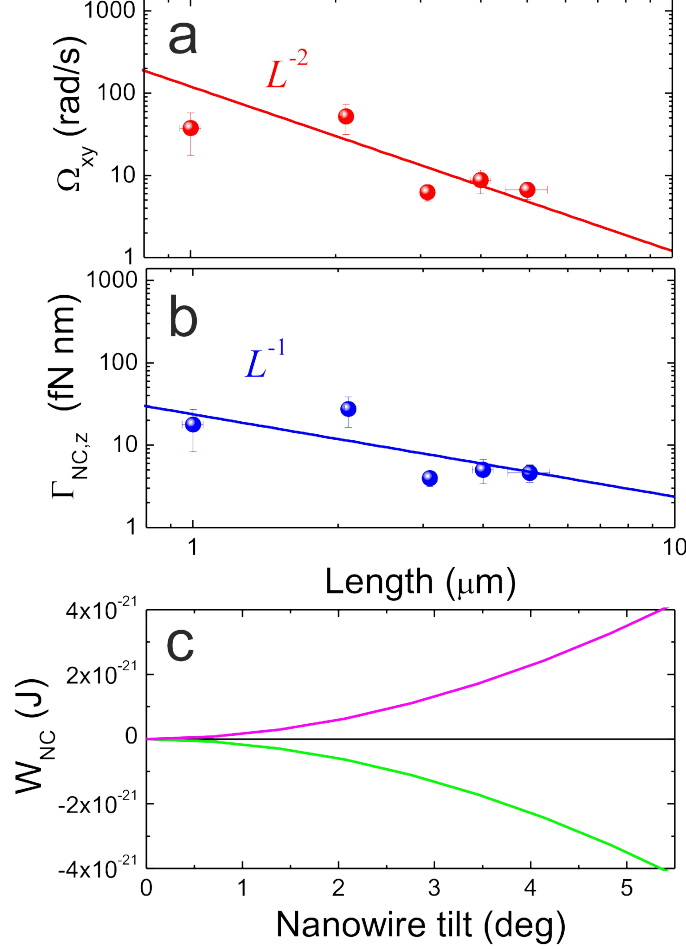


Figure 4: (a) Rotational frequency, Ω_{xy} , obtained from the DCCFs as a function of length, L . The red line is a fit to the data with a L^{-2} scaling law. The error bars represent the standard deviation from the mean value obtained over about 20 measurements for each length value on different trapped nanowires. The uncertainty on the length is obtained from scanning electron microscopy images of the as-prepared SiNW samples. (b) Scaling of the torque of the non-conservative force component as a function of SiNW length. The blue line is a fit to the data with a L^{-1} scaling law. (c) Calculation of the work done by a $4 \mu\text{m}$ SiNW as a function of its inclination and as translated in a circular path with radius equal to the measured transverse RMS displacement. The averaged tilt direction, φ , is fixed at 15 degrees with respect to the polarization (x -)axis. The calculations at small tilting are consistent (10^{-22} J) with the estimates obtained from the experiments.

trapping point and with a radius equal to the measured transverse RMS displacement, $\sqrt{\langle \rho^2 \rangle}$. An example of such calculations as a function of the wire inclination is shown in Fig. 4c. It is worth noting how the calculations at small (few degrees) tilting yield an estimate that is consistent (10^{-22} J) with the non-conservative work estimated from our measurements. Moreover, the persistent inclination and direction are dependent on the nanowire length as it is related to a balance between the restoring conservative torque of the OT and the non-conservative torque generated by the transverse components of the radiation force. **Finally, we point out that the work and power dissipated by the non-conservative force are related to the *external degrees-of-freedom* (center-of-mass, tilting) of the trapped particle. By Kohn's theorem⁶³ these are separated by the *internal degrees-of-freedom* to which energy is dissipated by heating effects²⁰ that for our experiments are estimated to be at the nanowatts level.**

In conclusion, non-conservative effects on non-spherical particles are linked to the occurrence of a transverse component of the radiation pressure. Although we measured non-conservative effects in the order of few percent of the trap strength **and with amplitudes in the range of 5-10%**, we were able to detect them at any available laser power **(up to 24 mW at the sample)**, so this needs to be taken into account when dealing with calibration of optical trapping forces based on effective potentials.^{18,64,65} **From our measurements we are not able to infer a possible power threshold at which non-conservative rotations disappear. However, recent experiments on thick tapered nanowires⁶⁶ show a change of behaviour of the non-conservative dynamics at about 50 mW. Further experimental work at higher power on ultrathin nanowires might be able to clarify if these effects truly disappear at some power or they just scale down monotonically.**

In addition, non-conservative forces can have a dramatic effect in optomechanics with levitated non-spherical particles.^{4,67} In this context, laser cooling of the particle motion relies on trapping in vacuum aiming to reach the quantum ground state of the effective harmonic potential and reveal quantum phenomena at the mesoscale.⁶⁸⁻⁷⁰ However, non-conservative forces may have a detrimental effect as they can strongly limit the cooling

efficiency and final center-of-mass effective temperature.⁷¹ Therefore, a careful consideration of non-conservative effects must be taken into account when undertaking laser cooling experiments on non-spherical particles.

Since completing this paper, Toe et al.⁶⁶ have published a study of the non-conservative dynamics of InP nanowires with a small taper in optical tweezers and presented a mechanical model for the rotational-translational coupling in the trap. The current work elucidates the origin of the non-conservative force in terms of a transverse component of the radiation pressure and its scaling with nanowire length, thereby highlighting the significance of symmetry and dimensionality in the occurrence of non-conservative effects in optical tweezers.

Supporting Information. The Supporting Information is available free of charge on the ACS Publications website. Silicon nanowires synthesis. Photonic torque microscopy and differential cross-correlations functions. DCCF and circulation. Stochastic circulation induced by transverse polarization forces. [Center-of-mass position and fluctuations.](#)

Acknowledgements. We acknowledge funding from MPNS COST Action 1205 “Advances in Optofluidics: Integration of Optical Control and Photonics with Microfluidics”. SHS acknowledges funding from the Czech Science Foundation (GB14-36681G).

References

- (1) Ashkin, A.; Dziedzic, J.; Bjorkholm, J.; Chu, S. *Opt. Lett.* **1986**, *11*, 288.
- (2) Jones, P. H.; Maragò, O. M.; Volpe, G. *Optical tweezers: Principles and applications*; Cambridge University Press: Cambridge, 2015.
- (3) Dholakia, K.; Čížmár, T. *Nature Photon.* **2011**, *5*, 335–342.
- (4) Maragò, O. M.; Jones, P. H.; Gucciardi, P. G.; Volpe, G.; Ferrari, A. C. *Nat. Nanotech.* **2013**, *8*, 807–819.

- (5) Agarwal, R.; Ladavac, K.; Roichman, Y.; Yu, G.; Lieber, C.; Grier, D. *Opt. Express* **2005**, *13*, 8906–8912.
- (6) Maragò, O. M.; Gucciardi, P. G.; Bonaccorso, F.; Calogero, G.; Scardaci, V.; Rozhinc, A. G.; Ferrari, A. C.; Jones, P. H.; Saija, R.; Borghese, F.; Denti, P.; Iatì, M. A. *Physica E: Low-dimensional Systems and Nanostructures* **2008**, *40*, 2347 – 2351.
- (7) Neves, A. A. R.; Camposeo, A.; Pagliara, S.; Saija, R.; Borghese, F.; Denti, P.; Iatì, M. A.; Cingolani, R.; Maragò, O. M.; ; Pisignano, D. *Opt. Express* **2010**, *18*, 822–830.
- (8) Irrera, A.; Artoni, P.; Saija, R.; Gucciardi, P. G.; Iatì, M. A.; Borghese, F.; Denti, P.; Iacona, F.; Priolo, F.; ; Maragò, O. M. *Nano Lett.* **2011**, *11*, 4879–4884.
- (9) Yan, Z.; Jureller, J. E.; Sweet, J.; Guffey, M. J.; Pelton, M.; Scherer, N. F. *Nano Lett.* **2012**, *12*, 5155–5161.
- (10) Brzobohatý, O.; Šiler, M.; Trojek, J.; Chvátal, L.; Karásek, V.; Paták, A.; Pokorná, Z.; Mika, F.; Zemánek, P. *Sci. Rep.* **2015**, *5*.
- (11) Pauzauskie, P. J.; Radenovic, A.; Trepagnier, E.; Shroff, H.; Yang, P.; Liphardt, J. *Nat. Mater.* **2006**, *5*, 97–101.
- (12) Lee, S.-W.; Jo, G.; Lee, T.; Lee, Y.-G. *Opt. Express* **2009**, *17*, 17491–17501.
- (13) Reece, P. J.; Toe, W. J.; Wang, F.; Paiman, S.; Gao, Q.; Tan, H. H.; Jagadish, C. *Nano Lett.* **2011**, *11*, 2375–2381.
- (14) Wang, F.; Toe, W. J.; Lee, W. M.; McGloin, D.; Gao, Q.; Tan, H. H.; Jagadish, C.; Reece, P. J. *Nano Lett.* **2013**, *13*, 1185–1191.
- (15) Brzobohatý, O.; Šiler, M.; Trojek, J.; Chvátal, L.; Karásek, V.; Zemánek, P. *Opt. Express* **2015**, *23*, 8179–8189.

- (16) Nakayama, Y.; Pauzauskie, P. J.; Radenovic, A.; Onorato, R. M.; Saykally, R. J.; Liphardt, J.; Yang, P. *Nature* **2007**, *447*, 1098–1101.
- (17) Maragò, O. M.; Jones, P. H.; Bonaccorso, F.; Scardaci, V.; Gucciardi, P. G.; Rozhin, A.; Ferrari, A. C. *Nano Lett.* **2008**, *8*, 3211–3216.
- (18) Phillips, D.; Padgett, M.; Hanna, S.; Ho, Y.-L.; Carberry, D.; Miles, M.; Simpson, S. *Nature Photon.* **2014**, *8*, 400–405.
- (19) Dutto, F.; Raillon, C.; Schenk, K.; Radenovic, A. *Nano Lett.* **2011**, *11*, 2517–2521.
- (20) Roder, P. B.; Smith, B. E.; Davis, E. J.; Pauzauskie, P. J. *The Journal of Physical Chemistry C* **2014**, *118*, 1407–1416.
- (21) Smith, B. E.; Roder, P. B.; Zhou, X.; Pauzauskie, P. J. *Chem. Phys. Lett.* **2015**, *639*, 310–314.
- (22) Borghese, F.; Denti, P.; Saija, R.; Iati, M. A.; Maragò, O. M. *Phys. Rev. Lett.* **2008**, *100*, 163903.
- (23) Trojek, J.; Chvátal, L.; Zemánek, P. *JOSA A* **2012**, *29*, 1224–1236.
- (24) Simpson, S.; Hanna, S. *Nanotechnology* **2012**, *23*, 205502.
- (25) Priolo, F.; Gregorkiewicz, T.; Galli, M.; Krauss, T. F. *Nat. Nanotechnol.* **2014**, *9*, 19–32.
- (26) Smith, B. E.; Roder, P. B.; Hanson, J. L.; Manandhar, S.; Devaraj, A.; Perea, D. E.; Kim, W.-J.; Kilcoyne, A. D.; Pauzauskie, P. J. *ACS Photonics* **2015**, *2*, 559–564.
- (27) Arias-González, J. R.; Nieto-Vesperinas, M. *J. Opt. Soc. Am. A* **2003**, *20*, 1201–1209.
- (28) Albaladejo, S.; Marqués, M. I.; Laroche, M.; Sáenz, J. J. *Phys. Rev. Lett.* **2009**, *102*, 113602.

- (29) Ashkin, A. *Biophys. J.* **1992**, *61*, 569.
- (30) Callegari, A.; Mijalkov, M.; Gököz, A. B.; Volpe, G. *J. Opt. Soc. Am. B* **2015**, *32*, B11–B19.
- (31) Helmholtz, H. *Journal für die reine und angewandte Mathematik* **1858**, *55*, 25–55.
- (32) Merenda, F.; Boer, G.; Rohner, J.; Delacrétaz, G.; Salathé, R.-P. *Opt. Express* **2006**, *14*, 1685–1699.
- (33) Roichman, Y.; Sun, B.; Stolarski, A.; Grier, D. G. *Phys. Rev. Lett.* **2008**, *101*, 128301.
- (34) Saija, R.; Iatì, M. A.; Giusto, A.; Denti, P.; Borghese, F. *J. Quant. Spectrosc. Radiat. Transfer* **2005**, *94*, 163 – 179.
- (35) Bliokh, K. Y.; Bekshaev, A. Y.; Nori, F. *Nat. Commun.* **2014**, *5*, 3300.
- (36) Antognozzi, M.; Simpson, S.; Harniman, R.; Senior, J.; Hayward, R.; Hoerber, H.; Dennis, M. R.; Bekshaev, A. Y.; Bliokh, K. Y.; Nori, F. *Nature Physics* **2016**,
- (37) Iglesias, I.; Sáenz, J. J. *Opt. Commun.* **2011**, *284*, 2430–2436.
- (38) Pesce, G.; Volpe, G.; De Luca, A. C.; Rusciano, G.; Volpe, G. *EPL (Europhysics Letters)* **2009**, *86*, 38002.
- (39) Sun, B.; Lin, J.; Darby, E.; Grosberg, A. Y.; Grier, D. G. *Phys. Rev. E* **2009**, *80*, 010401.
- (40) Wu, P.; Huang, R.; Tischer, C.; Jonas, A.; Florin, E.-L. *Phys. Rev. Lett.* **2009**, *103*, 108101.
- (41) Borghese, F.; Denti, P.; Saija, R.; Iatì, M. A. *Opt. Express* **2007**, *15*, 11984–11998.
- (42) Saija, R.; Iatì, M.; Giusto, A.; Borghese, F.; Denti, P.; Aiello, S.; Cecchi-Pestellini, C. *Mon. Not. R. Astron. Soc.* **2003**, *341*, 1239–1245.

- (43) Swartzlander Jr, G. A.; Peterson, T. J.; Artusio-Glimpse, A. B.; Raisanen, A. D. *Nature Photon.* **2010**, *5*, 48–51.
- (44) Simpson, S. H.; Hanna, S.; Peterson, T. J.; Swartzlander, G. A. *Opt. Lett.* **2012**, *37*, 4038–4040.
- (45) Mihiretie, B. M.; Snabre, P.; Loudet, J. C.; Pouligny, B. *EPL (Europhysics Letters)* **2012**, *100*, 48005.
- (46) Mihiretie, B. M.; Snabre, P.; Loudet, J.-C.; Pouligny, B. *Eur. Phys. J. E Soft Matter* **2014**, *37*, 1–17.
- (47) Volpe, G.; Petrov, D. *Phys. Rev. Lett.* **2006**, *97*, 210603.
- (48) Irrera, A.; Artoni, P.; Iacona, F.; Pecora, E. F.; Franzo, G.; Galli, M.; Fazio, B.; Boninelli, S.; Priolo, F. *Nanotechnology* **2012**, *23*, 075204.
- (49) Huang, Z.; Geyer, N.; Werner, P.; De Boor, J.; Gösele, U. *Advanced Materials* **2011**, *23*, 285–308.
- (50) Fazio, B.; Artoni, P.; Iati, M. A.; D’Andrea, C.; Lo Faro, M. J.; Del Sorbo, S.; Pirotta, S.; Gucciardi, P. G.; Musumeci, P.; Vasi, C.; Saija, R.; Galli, M.; Priolo, F.; Irrera, A. *Light: Science & Applications* **2016**, *5*, e16062.
- (51) Haro-Gonzalez, P.; Del Rosal, B.; Maestro, L. M.; Rodriguez, E. M.; Naccache, R.; Capobianco, J. A.; Dholakia, K.; Solé, J. G.; Jaque, D. *Nanoscale* **2013**, *5*, 12192–12199.
- (52) Li, D.; Wu, Y.; Kim, P.; Shi, L.; Yang, P.; Majumdar, A. *Applied Physics Letters* **2003**, *83*, 2934–2936.
- (53) Gittes, F.; Schmidt, C. F. *Opt. Lett.* **1998**, *23*, 7–9.

- (54) Pesce, G.; Volpe, G.; Maragò, O. M.; Jones, P. H.; Gigan, S.; Sasso, A.; Volpe, G. *J. Opt. Soc. Am. B* **2015**, *32*, B84–B98.
- (55) Griesshammer, M.; Rohrbach, A. *Optics Express* **2014**, *22*, 6114–6132.
- (56) Simpson, S. H.; Hanna, S. *Phys. Rev. E* **2010**, *82*, 031141.
- (57) Jones, P. H.; Palmisano, F.; Bonaccorso, F.; Gucciardi, P. G.; Calogero, G.; Ferrari, A. C.; Maragò, O. M. *ACS Nano* **2009**, *3*, 3077–3084.
- (58) Volpe, G.; Volpe, G.; Petrov, D. *Phys. Rev. E* **2007**, *76*, 061118.
- (59) Tirado, M. M.; Martinez, C. L.; de la Torre, J. G. *J. Chem. Phys.* **1984**, *81*, 2047–2052.
- (60) Bryant, Z.; Stone, M. D.; Gore, J.; Smith, S. B.; Cozzarelli, N. R.; Bustamante, C. *Nature* **2003**, *424*, 338–341.
- (61) Berry, R. M.; Berg, H. C. *Proc. Natl. Acad. Sci. U.S.A* **1997**, *94*, 14433–14437.
- (62) Ozin, G. A.; Manners, I.; Fournier-Bidoz, S.; Arsenault, A. *Advanced Materials* **2005**, *17*, 3011–3018.
- (63) Lipparini, E. *Modern Many-Particle Physics*; World Scientific: Singapore.
- (64) Phillips, D.; Gibson, G.; Bowman, R.; Padgett, M.; Hanna, S.; Carberry, D.; Miles, M.; Simpson, S. *Opt. Express* **2012**, *20*, 29679–29693.
- (65) Bui, A. A.; Stilgoe, A. B.; Nieminen, T. A.; Rubinsztein-Dunlop, H. *Opt. Lett.* **2013**, *38*, 1244–1246.
- (66) Toe, W. J.; Ortega-Piwonka, I.; Angstmann, C. N.; Gao, Q.; Tan, H. H.; Jagadish, C.; Henry, B. I.; Reece, P. J. *Phys. Rev. E* **2016**, *93*, 022137.
- (67) Kuhn, S.; Asenbaum, P.; Kosloff, A.; Sclafani, M.; Stickler, B. A.; Nimmrichter, S.; Hornberger, K.; Cheshnovsky, O.; Patolsky, F.; Arndt, M. *Nano Lett.* **2015**, *15*, 5604–5608.

- (68) Gieseler, J.; Deutsch, B.; Quidant, R.; Novotny, L. *Phys. Rev. Lett.* **2012**, *109*, 103603.
- (69) Kiesel, N.; Blaser, F.; Delić, U.; Grass, D.; Kaltenbaek, R.; Aspelmeyer, M. *Proc. Natl. Acad. Sci. U.S.A* **2013**, *110*, 14180–14185.
- (70) Millen, J.; Fonseca, P.; Mavrogordatos, T.; Monteiro, T.; Barker, P. *Phys. Rev. Lett.* **2015**, *114*, 123602.
- (71) Divitt, S.; Rondin, L.; Novotny, L. *Opt. Lett.* **2015**, *40*, 1900–1903.